

A fractional-order chaotic Lorenz-based chemical system: Dynamic investigation, complexity analysis, chaos synchronization, and its application to secure communication

Haneche Nabil, and Hamaizia Tayeb

Citation: Chin. Phys. B, 2024, 33 (**12**): 120503. DOI: 10.1088/1674-1056/ad7fcf
Journal homepage: http://cpb.iphy.ac.cn; http://iopscience.iop.org/cpb

What follows is a list of articles you may be interested in

A color image encryption scheme based on a 2D coupled chaotic system and diagonal scrambling algorithm

Jingming Su(苏静明), Shihui Fang(方士辉), Yan Hong(洪炎), and Yan Wen(温言)
Chin. Phys. B, 2024, 33 (**7**): 070502. DOI: 10.1088/1674-1056/ad3efa

Two-dimensional-lag complex logistic map with complex parameters and its encryption application

Fangfang Zhang(张芳芳), Jinbo Wu(武金波), Lei Kou(寇磊), Fengying Ma(马凤英), Liming Wu(吴黎明), and Xue Zhang(张雪)
Chin. Phys. B, 2024, 33 (**5**): 050505. DOI: 10.1088/1674-1056/ad2a69

Remote sensing image encryption algorithm based on novel hyperchaos and an elliptic curve cryptosystem

Jing-Xi Tian(田婧希), Song-Chang Jin(金松昌), Xiao-Qiang Zhang(张晓强), Shao-Wu Yang(杨绍武), and Dian-Xi Shi(史殿习)
Chin. Phys. B, 2024, 33 (**5**): 050502. DOI: 10.1088/1674-1056/ad20d9

A lightweight symmetric image encryption cryptosystem in wavelet domain based on an improved sine map

Baichi Chen(陈柏池), Linqing Huang(黄林青), Shuting Cai(蔡述庭), Xiaoming Xiong(熊晓明), and Hui Zhang(张慧)
Chin. Phys. B, 2024, 33 (**3**): 030501. DOI: 10.1088/1674-1056/ad1030

Multiple mixed state variable incremental integration for reconstructing extreme multistability in a novel memristive hyperchaotic jerk system with multiple cubic nonlinearity

Meng-Jiao Wang(王梦蛟) and Lingfang Gu(辜玲芳)
Chin. Phys. B, 2024, 33 (**2**): 020504. DOI: 10.1088/1674-1056/acddd0

A fractional-order chaotic Lorenz-based chemical system: Dynamic investigation, complexity analysis, chaos synchronization, and its application to secure communication

Haneche Nabil[1,†] and Hamaizia Tayeb[2]

[1] *Mathematical Modeling & Simulation Laboratory, Department of Mathematics, University of Mentouri Brothers, Constantine, Algeria*
[2] *Department of Mathematics, University of Mentouri Brothers, Constantine, Algeria*

(Received 12 August 2024; revised manuscript received 14 September 2024; accepted manuscript online 26 September 2024)

Synchronization of fractional-order chaotic systems is receiving significant attention in the literature due to its applications in a variety of fields, including cryptography, optics, and secure communications. In this paper, a three-dimensional fractional-order chaotic Lorenz model of chemical reactions is discussed. Some basic dynamical properties, such as stability of equilibria, Lyapunov exponents, bifurcation diagrams, Poincaré map, and sensitivity to initial conditions, are studied. By adopting the Adomian decomposition algorithm (ADM), the numerical solution of the fractional-order system is obtained. It is found that the lowest derivative order in which the proposed system exhibits chaos is $q = 0.694$ by applying ADM. The result has been validated by the existence of one positive Lyapunov exponent and by employing some phase diagrams. In addition, the richer dynamics of the system are confirmed by using powerful tools in nonlinear dynamic analysis, such as the 0–1 test and C_0 complexity. Moreover, modified projective synchronization has been implemented based on the stability theory of fractional-order systems. This paper presents the application of the modified projective synchronization in secure communication, where the information signal can be transmitted and recovered successfully through the channel. MATLAB simulations are provided to show the validity of the constructed secure communication scheme.

Keywords: chaotic system, Adomian decomposition method, modified projective synchronization, secure communication

PACS: 05.45.–a, 05.45.Gg, 05.45.Pq, 05.45.Vx **DOI:** 10.1088/1674-1056/ad7fcf

1. Introduction

Fractional calculus is an important topic in modern mathematics that generalizes the classical calculus, including integrals and derivatives of arbitrary order. In fact, fractional calculus tools have become widely used to understand real-world phenomena that are modeled with non-integer-order derivatives. The applications of fractional calculus have increased in many different areas, including biology,[1] medicine,[2] physics,[3] chemistry,[4] finance,[5] signal processing,[6] control theory,[7] optimization,[8] chaos theory,[9] and many others. To our knowledge, Leibniz explored the first idea of the fractional derivative in his works in 1695.[10] Later, several types of fractional derivatives have been discovered, with and without singular kernels. With singular kernels, we have the well-known Caputo derivative and Riemann–Liouville derivative.[11] Without singular kernels, we have the Caputo–Fabrizio derivative,[12] which is known as fractional derivative with exponential kernel, and the Atangana–Baleanu derivative,[13] which is known as fractional derivative with Mittag–Leffler kernel. In particular, fractional calculus has several significant applications in chemical systems. For example, fractional calculus is used to design advanced controllers that enhance the performance of the traditional controllers in certain chemical processes. These controllers have the advantage of improving the stability of irregular motions in chemical systems. On the other hand, fractional calculus aids in accurately modeling mass transfer in various adsorption processes, thereby significantly enhancing their prediction and optimization. In addition, fractional derivatives can display what is called the "memory effect", where the current state depends on past states over a long period. This can aid chemists in comprehending the behaviors of various systems more precisely because fractional calculus plays a crucial role in modeling complex systems with memory and hereditary properties, which are very common in nonlinear chemical systems.[14] The Caputo fractional derivative is often chosen for modeling chemical and biological systems due to several key advantages. First, the Caputo derivative incorporates memory effects, which are critical for accurate phenomenon modeling where the current state depends on the system's history. Second, it allows for more flexible modeling of complex dynamics compared to integer-order derivatives due to its compatibility with classical initial conditions typically used in real-world systems.[15] In particular, it helps us to better describe the behaviors observed in chemical reactions. Furthermore, the Caputo derivative provides stability, accuracy, and smoothness in numerical simulations for solving complex systems in chemistry and biology.

In recent decades, nonlinear systems have been studied

†Corresponding author. E-mail: nabil.haneche@doc.umc.edu.dz

© 2024 Chinese Physical Society and IOP Publishing Ltd

and developed due to their sensitivity to both parameter values and initial conditions. A small change in the system parameters or initial conditions can lead to completely different outcomes, which is known as chaos phenomena.[16] A chaotic system is a deterministic nonlinear system that has at least one positive Lyapunov exponent.[17] In the chaos literature, there is a significant interest shown in the study of chaotic dynamical systems, particularly physics and chemistry. In physics, the authors in Ref. [18] have studied the Rucklidge chaotic system, which is similar to the Lorenz system, which is a three-dimensional model of a double convection process. In Ref. [19], Aqeel *et al*. have investigated the chaotic dynamics of the Krause and Robert (KR) system, which is a simple mathematical model of the Rikitake two-disc dynamo geomagnetic system. In chemistry, Bodale *et al*. have investigated in Ref. [20] the chaos control for the Willamowski–Rössler model of chemical reactions. In addition, they achieved a chaos synchronization for two Willamowski–Rössler systems with the aim of determining the suitable conditions for a practical implementation of this synchronization. In Ref. [21], Yadav *et al*. presented a three-dimensional fractional-order chaotic chemical reactor system. This model has been investigated using the Lyapunov stability theory of fractional-order systems, stability analysis, chaos control, and chaos synchronization. For more mathematical models of chaotic systems in physics and chemistry, see Refs. [22–25].

Since the works of Pecora and Carroll in 1990,[26] the synchronization of chaotic systems has gained significant attention in the last few years due to its potential applications in secure communications and signal processing. In the synchronization of chaotic systems, we consider a pair of identical or different chaotic systems, known as the drive and response systems, for the synchronization process. By adopting a suitable controller, the state trajectories of the response systems asymptotically track the state trajectories of the drive system in infinite time. From the literature survey, various types of chaotic synchronizations have been introduced, such as complete synchronization,[27] where the difference of states of the synchronized systems converges to zero for a large time, anti-synchronization,[28] projective synchronization,[29] generalized synchronization,[30] phase synchronization,[31] lag synchronization,[32] etc. In recent years, a new kind of chaotic synchronization has been introduced called function projective synchronization (FPS),[33] where two identical or different chaotic systems could be synchronized up to a scaling function. Furthermore, in Ref. [34] Du *et al*. proposed a new kind of synchronization, which is the modified function projective synchronization (MFPS), where the drive and response systems could be synchronized up to a scaling function matrix. In Ref. [35], Li proposed the modified projective synchronization (MPS) of chaotic systems, where the drive and response systems could be synchronized up to a constant scaling matrix. According to our understanding, the application of the scaling matrix in secure communication can enhance the security level of the scheme. Motivated by the above discussion, it is useful to study MPS of chaotic systems and apply it to secure communication.

Given that the derivative order can be viewed as an additional system parameter and that a chaotic system is sensitive to variations in its parameters and derivative order, the application of fractional-order chaotic systems in secure communication schemes can offer greater security and accuracy compared to integer-order systems. The main idea of transmitting an information signal using chaotic systems is to inject the message into a chaotic signal, hide this information via a public channel, and then send it to the receiver system. Finally, when the synchronization of the transmitter and receiver systems is achieved, the original message can be successfully recovered at the receiver. From a mathematical perspective, researchers have studied and used various fractional-order chaotic systems to achieve secure communication.[36–39] Three types based on chaos have been proposed to realize a secure communication scheme, including chaotic masking,[40] chaotic modulation,[41] and chaotic shift keying.[42] In chaotic masking, the original message is added to a chaotic signal, which is then transmitted to the receiver. In chaotic modulation, the original message is either injected into one of the states or system parameters, or it is modulated by introducing an invertible function. When the transmitter and receiver systems are synchronized, the information signal can be recovered at the receiver. In the chaotic shift keying technique, a chaotic system generates a chaotic signal, which serves as the carrier wave. The information to be transmitted is viewed as binary data, which modulates the chaotic signal. The information signal can be recovered at the receiver after the synchronization between the transmitter and receiver systems. In this work, the chaotic modulation technique is used to achieve a secure communication scheme.

The rest of this work is planned as follows. Section 2 presents basic notions related to fractional calculus. Based on ADM algorithm, Section 3 deals with the numerical solution of the proposed fractional-order system and then the stability of equilibrium points is analyzed. In Section 4, the dynamical properties of the fractional-order system are studied by means of powerful tools in the nonlinear dynamic analysis. In Section 5, the complexity of the proposed fractional-order system is measured by adopting the 0–1 test and C_0 complexity algorithms. Section 6 focuses on the MPS of the fractional-order chaotic systems. In Section 7, a secure communication scheme based on the MPS of fractional-order chaotic systems is constructed. We draw conclusions in Section 8.

2. Mathematical background

This section presents some basic notions of fractional calculus that will aid the reader to understand the content of this paper.

Definition 1 The Riemann–Liouville fractional integral of order $q \in \mathbb{R}^+$ of a continuous function $\xi : \mathbb{R}^+ \to \mathbb{R}$ is defined as[43]

$$J_{t_0}^q \xi(t) = \frac{1}{\Gamma(q)} \int_{t_0}^{t} (t-u)^{q-1} \xi(u) \mathrm{d}u, \tag{1}$$

where $t > t_0$, $\Gamma(\cdot)$ is the Euler Gamma function.

For $\gamma > -1$ and C is a given real constant, we have the following properties of the fractional integral operator $J_{t_0}^q$:

$$\begin{aligned} &J_{t_0}^0 \xi(t) = \xi(t), \\ &J_{t_0}^q (t-t_0)^\gamma = \frac{\Gamma(\gamma+1)}{\Gamma(\gamma+1+q)} (t-t_0)^{\gamma+q}, \\ &J_{t_0}^q C = \frac{C}{\Gamma(q+1)} (t-t_0)^q. \end{aligned} \tag{2}$$

Definition 2 The Caputo fractional derivative of order $q \in \mathbb{R}^+$ of a continuous function $\xi : [t_0, +\infty[\to \mathbb{R}$ is defined as[44]

$${}^c D_{t_0}^q \xi(t) = \frac{1}{\Gamma(m-q)} \int_{t_0}^{t} \frac{\xi^{(m)}(u)}{(t-u)^{q+1-m}} \mathrm{d}u, \tag{3}$$

where $t > t_0$, $m-1 < q \le m$ with $m = \lceil q \rceil$.

Two fundamental properties of the Caputo differential operator are given as follows:

$$\begin{aligned} {}^c D_{t_0}^q J_{t_0}^q \xi(t) &= \xi(t), \\ J_{t_0}^q ({}^c D_{t_0}^q) \xi(t) &= J_{t_0}^q J_{t_0}^{m-q} D_{t_0}^m \xi(t) \\ &= J_{t_0}^m D_{t_0}^m \xi(t) \\ &= \xi(t) - \sum_{n=0}^{m-1} \xi^{(n)}(t_0^+) \frac{(t-t_0)^n}{n!}. \end{aligned} \tag{4}$$

2.1. Adomian decomposition algorithm

Generally, a fractional-order nonlinear system can be divided into three parts

$${}^c D_{t_0}^q \xi(t) = L\xi(t) + N\xi(t) + h(t), \tag{5}$$

where $\xi(t) = [\xi_1(t), \xi_2(t), \ldots, \xi_n(t)]^{\mathrm{T}}$ is the system state variables. We denote by $L\xi(t)$ and $N\xi(t)$ the linear and nonlinear terms in the fractional-order system, respectively. Here, $h(t) = [h_1(t), h_2(t), \ldots, h_n(t)]^{\mathrm{T}}$ is the constant term of the system. We take the initial conditions as $\xi^{(k)}(t_0^+) = b_k = [\xi_1(t_0), \xi_2(t_0), \ldots, \xi_n(t_0)]^{\mathrm{T}}$, $k = 0, 1, \ldots, m-1$, $m \in \mathbb{N}$, $m-1 < q \le m$. By applying the fractional integral operator $J_{t_0}^q$ to both sides of Eq. (5), the following equation is obtained:[45]

$$\xi(t) = J_{t_0}^q L\xi(t) + J_{t_0}^q N\xi(t) + J_{t_0}^q h(t) + \phi, \tag{6}$$

where $\phi = \sum_{k=0}^{m-1} b_k \frac{(t-t_0)^k}{k!}$.

By adopting the following decomposition items:

$$\begin{aligned} \xi^0 &= \sum_{k=0}^{m-1} b_k \frac{(t-t_0)^k}{k!} + \phi, \\ \xi^1 &= J_{t_0}^q L\xi^0 + J_{t_0}^q A^0(\xi^0), \\ \xi^2 &= J_{t_0}^q L\xi^1 + J_{t_0}^q A^1(\xi^0, \xi^1), \\ &\vdots \\ \xi^i &= J_{t_0}^q L\xi^{i-1} + J_{t_0}^q A^{i-1}(\xi^0, \xi^1, \ldots, \xi^{i-1}), \\ &\vdots \end{aligned} \tag{7}$$

the exact solution of the fractional-order system is obtained as

$$\xi = \sum_{j=0}^{\infty} \xi^j = J_{t_0}^q \sum_{j=0}^{\infty} \xi^j + J_{t_0}^q \sum_{j=0}^{\infty} A^j + J_{t_0}^q \xi + \phi, \tag{8}$$

where A^j is the Adomian polynomial, which is calculated as[46]

$$A^j = \frac{1}{j!} \left[\frac{\mathrm{d}^j}{\mathrm{d}\lambda^j} N\left(\sigma_i^j(\lambda)\right) \right]_{\lambda=0}, \tag{9}$$

where $\sigma_i^j(\lambda) = \sum_{k=0}^{j} (\lambda)^k \xi_i^k$, $j = 0, 1, \ldots, \infty$ and $i = 1, 2, \ldots, n$. The nonlinear terms are expressed as

$$N\xi = \sum_{j=0}^{\infty} A^j(\xi^0, \xi^1, \ldots, \xi^j). \tag{10}$$

In practice, it is impossible to compute an infinite number of terms to obtain the exact solution of Eq. (5). So, we compute only the first terms with this method, because the ADM algorithm converges quickly.[47]

3. System description, numerical solution, and stability of equilibria

3.1. Mathematical model

The classical Lorenz dynamical system is described by the following dynamics:[48]

$$\begin{cases} \dot{X} = \sigma(Y - X), \\ \dot{Y} = \rho X - Y - XZ, \\ \dot{Z} = XY - \beta Z, \end{cases} \tag{11}$$

where X, Y, and Z are three species, and σ, ρ, and β are positive constant parameters. When the parameters are set as $\sigma = 10$, $\rho = 28$, and $\beta = 8/3$, the Lorenz system (11) exhibits a strange chaotic attractor. It is noted that in system (11), X and Y take both positive and negative values but Z remains positive. For chemical considerations, to keep X and Y always in the positive quadrant, we consider the following transformation:

$$x = X + a, \quad y = Y + a, \quad z = Z, \tag{12}$$

then system (11) becomes

$$\begin{cases} \dot{x} = \sigma(y - x), \\ \dot{y} = \rho x - y + az - xz - a(\rho - 1), \\ \dot{z} = -ax - ay - \beta z + xy + a^2. \end{cases} \tag{13}$$

When the parameter a is selected as $a = 30$, the Lorenz chaotic attractor is centered in the positive quadrant. From the chemical point of view, four categories can be used to classify the Lorenz-based chemical reactions: irreversible source reactions S, cooperative catalytic species of constant concentration C, irreversible deletion to an external sink E, and rate limiting (slow/fast) R. The slow and fast consecutive reactions can be described by the following relations:[49]

$$\begin{cases} D+x+z \longrightarrow D^*+x+z \quad \text{(slow)}, \\ D^*+y \longrightarrow D+R \quad \text{(fast)}, \end{cases} \tag{14}$$

where x and y act as catalysts to produce D^*, which is an activated form of species D that is thought to have a large and constant concentration. If we denote by A, B, etc, the species of constant concentration, the required reactions are given by the following relations:

$$\begin{aligned}
&(S): R \xrightarrow{\alpha_{12}} z, \quad JS = \alpha_{12}, \\
&(C_1): A+y \xrightarrow{\alpha_2} x+y, \quad JC_1 = y\alpha_2, \\
&(C_2): B+x \xrightarrow{\alpha_3} y+x, \quad JC_2 = x\alpha_3, \\
&(C_3): B+z \xrightarrow{\alpha_5} y+z, \quad JC_3 = z\alpha_5, \\
&(C_4): C+x+y \xrightarrow{\alpha_{11}} z+x+y, \quad JC_4 = xy\alpha_{11}, \\
&(R_1): D+x+z \xrightarrow[\text{(slow)}]{\alpha_6} D^*+x+z, \\
&\qquad D^*+y \xrightarrow[\text{(fast)}]{} D+R, \quad JR_1 = xz\alpha_6, \\
&(R_2): D \xrightarrow[\text{(slow)}]{\alpha_7} D^*, \\
&\qquad D^*+y \xrightarrow[\text{(fast)}]{} D+R, \quad JR_2 = \alpha_7, \\
&(R_3): E+x \xrightarrow[\text{(slow)}]{\alpha_8} E^*+x, \\
&\qquad E^*+z \xrightarrow[\text{(fast)}]{} E+R, \quad JR_3 = x\alpha_8, \\
&(R_4): E+y \xrightarrow[\text{(slow)}]{\alpha_9} E^*+y, \\
&\qquad E^*+z \xrightarrow[\text{(fast)}]{} E+R, \quad JR_4 = y\alpha_9, \\
&(E_1): x \xrightarrow{\alpha_1} R, \quad JE_1 = x\alpha_1, \\
&(E_2): y \xrightarrow{\alpha_4} R, \quad JE_2 = y\alpha_4, \\
&(E_3): z \xrightarrow{\alpha_{10}} R, \quad JE_3 = z\alpha_{10},
\end{aligned} \tag{15}$$

where α_j $(j = 1,2,\ldots,12)$ are rate constants and related to the Lorenz equations.

The following dynamical system is governed by these reactions in terms of constant rates J:

$$\begin{cases} \dot{x} = JC_1 - JE_1, \\ \dot{y} = JC_2 - JE_2 + JC_3 - JR_1 + JR_2, \\ \dot{z} = -JR_3 - JR_4 - JE_3 + JC_4 + JS. \end{cases} \tag{16}$$

Substituting the rates of relations (15) into the right side of equations (16), we obtain the following dynamical system:

$$\begin{cases} \dot{x} = \alpha_2 y - \alpha_1 x, \\ \dot{y} = \alpha_3 x - \alpha_4 y + \alpha_5 z - \alpha_6 xz + \alpha_7, \\ \dot{z} = -\alpha_8 x - \alpha_9 y - \alpha_{10} z + \alpha_{11} xy + \alpha_{12}, \end{cases} \tag{17}$$

where α_j $(j = 1,2,\ldots,12)$ are constant rates, and x, y, and z are the concentrations of species X, Y, and Z, respectively. Under the system parameters listed in Table 1 and the initial conditions $(x_0, y_0, z_0) = (32, 32, 32)$, the integer-order system (17) exhibits chaotic behavior. The double-scroll chaotic attractor of system (17) is shown in Fig. 1.

Table 1. Parameter values of the Lorenz-based chemical system (17).

Parameter	Value	Parameter	Value
α_1	10	α_7	-810
α_2	10	α_8	30
α_3	28	α_9	35.5
α_4	1	α_{10}	8/3
α_5	30	α_{11}	1
α_6	1	α_{12}	900

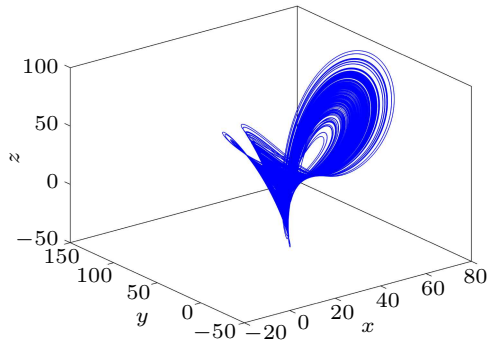


Fig. 1. Chaotic attractor of the integer-order Lorenz-based chemical system (17) in x–y–z space.

The significance of chaos in the Lorenz chemical system is to help us understand the complex dynamic behaviors in chemical reactions where the system can display rich nonlinear dynamics originally developed to model atmospheric convection. From a chemical perspective, nonlinear dynamics can describe how certain reactions evolve over time, particularly under nonequilibrium conditions. Furthermore, because the Lorenz system is dissipative, the chemical reactions occur in an open system where energy and matter are exchanged over time. Thus, the Lorenz system serves as an example of how dissipative systems can exhibit chaotic behavior, where even a small change in initial conditions can result in vastly different behaviors. This property helps chemists understand how energy dissipation and entropy changes can be affected by the chaotic behavior in the Lorenz chemical system. Hence, chemists can develop better predictive models for complex reactions by studying chaotic systems. Our contribution is to study the previous chemical model in its fractional-order counterpart in order to investigate its richer dynamic properties and achieve a chaos synchronization. Hence, by taking the fractional derivative operator on system (17), we obtain the following three-dimensional fractional-order Lorenz-based chemical system:

$$\begin{cases} {}^{c}D^{q}_{t_0} x = \alpha_2 y - \alpha_1 x, \\ {}^{c}D^{q}_{t_0} y = \alpha_3 x - \alpha_4 y + \alpha_5 z - \alpha_6 xz + \alpha_7, \\ {}^{c}D^{q}_{t_0} z = -\alpha_8 x - \alpha_9 y - \alpha_{10} z + \alpha_{11} xy + \alpha_{12}, \end{cases} \tag{18}$$

where x, y, and z are the state variables, α_j $(j=1,2,\ldots,12)$ are constant parameters, and ${}^{c}D_{t_0}^{q}$ is the Caputo fractional derivative with order $q\in(0,1]$. Applying ADM algorithm described in Section 2, the discrete iterative formula of the fractional-order Lorenz-based chemical system (18) is obtained as

$$\begin{aligned}
x_{m+1} &= x_m+(\alpha_2 y_m-\alpha_1 x_m)\frac{h^q}{\Gamma(q+1)}+[\alpha_2(\alpha_3 x_m-\alpha_4 y_m+\alpha_5 z_m-\alpha_6 x_m z_m+\alpha_7)+\cdots]\frac{h^{2q}}{\Gamma(2q+1)}+\cdots,\\
y_{m+1} &= y_m+[\alpha_3 x_m-\alpha_4 y_m+\alpha_5 z_m-\alpha_6 x_m z_m+\alpha_7]\frac{h^q}{\Gamma(q+1)}\\
&\quad+[\alpha_3(\alpha_2 y_m-\alpha_1 x_m)-\alpha_4(\alpha_3 x_m-\alpha_4 y_m+\alpha_5 z_m-\alpha_6 x_m z_m+\alpha_7)+\cdots]\frac{h^{2q}}{\Gamma(2q+1)}+\cdots,\\
z_{m+1} &= z_m+[-\alpha_8 x_m-\alpha_9 y_m-\alpha_{10} z_m+\alpha_{11} x_m y_m+\alpha_{12}]\frac{h^q}{\Gamma(q+1)}\\
&\quad+[-\alpha_8(\alpha_2 y_m-\alpha_1 x_m)-\alpha_9(\alpha_3 x_m-\alpha_4 y_m+\alpha_5 z_m-\alpha_6 x_m z_m+\alpha_7)+\cdots]\frac{h^{2q}}{\Gamma(2q+1)}+\cdots,
\end{aligned}\tag{19}$$

where h is iteration step size. As we said about the fast convergence of the ADM algorithm, we only calculate the six first terms as follows:

$$\begin{aligned}
c_1^0 &= x_m,\\
c_2^0 &= y_m+J_{t_0}^q(\alpha_7)=y_m+\frac{\alpha_7}{\Gamma(q+1)}(t-t_0)^q,\\
c_3^0 &= z_m+J_{t_0}^q(\alpha_{12})=z_m+\frac{\alpha_{12}}{\Gamma(q+1)}(t-t_0)^q;
\end{aligned}\tag{20}$$

$$\begin{aligned}
c_1^1 &= \alpha_2 c_2^0-\alpha_1 c_1^0,\\
c_2^1 &= \alpha_3 c_1^0-\alpha_4 c_2^0+\alpha_5 c_3^0-\alpha_6 c_1^0 c_3^0,\\
c_3^1 &= -\alpha_8 c_1^0-\alpha_9 c_2^0-\alpha_{10} c_3^0+\alpha_{11} c_1^0 c_2^0;
\end{aligned}\tag{21}$$

$$\begin{aligned}
c_1^2 &= \alpha_2 c_2^1-\alpha_1 c_1^1,\\
c_2^2 &= \alpha_3 c_1^1-\alpha_4 c_2^1+\alpha_5 c_3^1-\alpha_6\left(c_1^1 c_3^0+c_1^0 c_3^1\right),\\
c_3^2 &= -\alpha_8 c_1^1-\alpha_9 c_2^1-\alpha_{10} c_3^1+\alpha_{11}\left(c_1^1 c_2^0+c_1^0 c_2^1\right);
\end{aligned}\tag{22}$$

$$\begin{aligned}
c_1^3 &= \alpha_2 c_2^2-\alpha_1 c_1^2,\\
c_2^3 &= \alpha_3 c_1^2-\alpha_4 c_2^2+\alpha_5 c_3^2\\
&\quad-\alpha_6\left(c_1^0 c_3^2+\frac{\Gamma(2q+1)}{\Gamma^2(q+1)}c_1^1 c_3^1+c_1^2 c_3^0\right),\\
c_3^3 &= -\alpha_8 c_1^2-\alpha_9 c_2^2-\alpha_{10} c_3^2\\
&\quad+\alpha_{11}\left(c_1^0 c_2^2+\frac{\Gamma(2q+1)}{\Gamma^2(q+1)}c_1^1 c_2^1+c_1^2 c_2^0\right);
\end{aligned}\tag{23}$$

$$\begin{aligned}
c_1^4 &= \alpha_2 c_2^3-\alpha_1 c_1^3,\\
c_2^4 &= \alpha_3 c_1^3-\alpha_4 c_2^3+\alpha_5 c_3^3\\
&\quad-\alpha_6\left(c_1^0 c_3^3+\frac{\Gamma(3q+1)}{\Gamma(q+1)\Gamma(2q+1)}(c_1^1 c_3^2+c_1^2 c_3^1)+c_1^3 c_3^0\right),\\
c_3^4 &= -\alpha_8 c_1^3-\alpha_9 c_2^3-\alpha_{10} c_3^3\\
&\quad+\alpha_{11}\left(c_1^0 c_2^3+\frac{\Gamma(3q+1)}{\Gamma(q+1)\Gamma(2q+1)}(c_1^1 c_2^2+c_1^2 c_2^1)+c_1^3 c_2^0\right);
\end{aligned}\tag{24}$$

$$\begin{aligned}
c_1^5 &= \alpha_2 c_2^4-\alpha_1 c_1^4,\\
c_2^5 &= \alpha_3 c_1^4-\alpha_4 c_2^4+\alpha_5 c_3^4\\
&\quad-\alpha_6\left(c_1^0 c_3^4+\frac{\Gamma(4q+1)}{\Gamma(q+1)\Gamma(3q+1)}(c_1^1 c_3^3+c_1^3 c_3^1)\right.\\
&\quad\left.+\frac{\Gamma(4q+1)}{\Gamma^2(2q+1)}c_1^2 c_3^2+c_1^4 c_3^0\right),\\
c_3^5 &= -\alpha_8 c_1^4-\alpha_9 c_2^4-\alpha_{10} c_3^4\\
&\quad+\alpha_{11}\left(c_1^0 c_2^4+\frac{\Gamma(4q+1)}{\Gamma(q+1)\Gamma(3q+1)}(c_1^1 c_3^3+c_1^3 c_2^1)\right.\\
&\quad\left.+\frac{\Gamma(4q+1)}{\Gamma^2(2q+1)}c_1^2 c_2^2+c_1^0 c_2^4\right);
\end{aligned}\tag{25}$$

$$\begin{aligned}
c_1^6 &= \alpha_2 c_2^5-\alpha_1 c_1^5,\\
c_2^6 &= \alpha_3 c_1^5-\alpha_4 c_2^5+\alpha_5 c_3^5-\alpha_6(c_1^0 c_3^5\\
&\quad+\frac{\Gamma(5q+1)}{\Gamma(q+1)\Gamma(4q+1)}(c_1^1 c_3^4+c_1^4 c_3^1)\\
&\quad+\frac{\Gamma(5q+1)}{\Gamma(2q+1)\Gamma(3q+1)}(c_1^2 c_3^3+c_1^3 c_3^2)+c_1^5 c_3^0),\\
c_3^6 &= -\alpha_8 c_1^5-\alpha_9 c_2^5-\alpha_{10} c_3^5+\alpha_{11}(c_1^0 c_2^5\\
&\quad+\frac{\Gamma(5q+1)}{\Gamma(q+1)\Gamma(4q+1)}(c_1^1 c_2^4+c_1^4 c_2^1)\\
&\quad+\frac{\Gamma(5q+1)}{\Gamma(2q+1)\Gamma(3q+1)}(c_1^2 c_2^3+c_1^3 c_2^2)+c_1^5 c_2^0).
\end{aligned}\tag{26}$$

Thus, we can obtain

$$\begin{bmatrix} x_{m+1}\\ y_{m+1}\\ z_{m+1}\end{bmatrix}=\begin{bmatrix} c_1^0 & c_1^1 & c_1^2 & c_1^3 & c_1^4 & c_1^5 & c_1^6\\ c_2^0 & c_2^1 & c_2^2 & c_2^3 & c_2^4 & c_2^5 & c_2^6\\ c_3^0 & c_3^1 & c_3^2 & c_3^3 & c_3^4 & c_3^5 & c_3^6\end{bmatrix}\begin{bmatrix} 1 & \frac{h^q}{\Gamma(q+1)} & \frac{h^{2q}}{\Gamma(2q+1)} & \frac{h^{3q}}{\Gamma(3q+1)} & \frac{h^{4q}}{\Gamma(4q+1)} & \frac{h^{5q}}{\Gamma(5q+1)} & \frac{h^{6q}}{\Gamma(6q+1)}\end{bmatrix}^{\mathrm{T}}.\tag{27}$$

Based on the recursive formulas (27), the discrete counterpart of fractional-order Lorenz-based chemical system (18) is obtained. Thus, by adopting the chaotic sequences, we can easily investigate the qualitative characteristics of the chemical system.

3.2. Stability of equilibria

This subsection deals with the existence and stability analysis of the equilibrium points of fractional-order Lorenz-based chemical system (18). In order to investigate the stability of equilibrium points of fractional-order system, we consider the following commensurate fractional-order system:

$$ {}^{c}D_{t_0}^{q}X(t) = f(X), \quad X(0) = X_0, \tag{28}$$

where $0 < q \leq 1, X \in \mathbb{R}^n$.

Theorem 1[50] The commensurate fractional-order system (28) is asymptotically stable if and only if

$$ |\arg(\lambda)| > q\frac{\pi}{2}, \tag{29}$$

where λ is the eigenvalue of the Jacobian matrix $J = \partial f(X)/\partial X$ of system (28) evaluated at the equilibrium point E.

To provide further clarification, Fig. 2 shows the stability region of commensurate fractional-order system.

Fix the system parameters as mentioned in Table 1 and solve the following system of equations:

$$ \begin{cases} \alpha_2 y - \alpha_1 x = 0, \\ \alpha_3 x - \alpha_4 y + \alpha_5 z - \alpha_6 xz + \alpha_7 = 0, \\ -\alpha_8 x - \alpha_9 y - \alpha_{10} z + \alpha_{11} xy + \alpha_{12} = 0. \end{cases} \tag{30}$$

We find that the system (18) has three equilibrium points: $E_1 = (30,30,0)$, $E_2 = (21.514,21.514,27)$, and $E_3 = (38.485,38.485,27)$. By linearization around the equilibria $E^* = (x^*,y^*,z^*)$, the Jacobian matrix of system (18) is given by

$$ J_{E^*} = \begin{pmatrix} -\alpha_1 & \alpha_2 & 0 \\ \alpha_3 - \alpha_6 z^* & -\alpha_4 & \alpha_5 - \alpha_6 x^* \\ -\alpha_8 + \alpha_{11} y^* & -\alpha_9 + \alpha_{11} x^* & -\alpha_{10} \end{pmatrix}. \tag{31}$$

According to the stability criterion of the fractional-order dynamical systems (1), the stability of equilibria of system (18) is shown in Table 2.

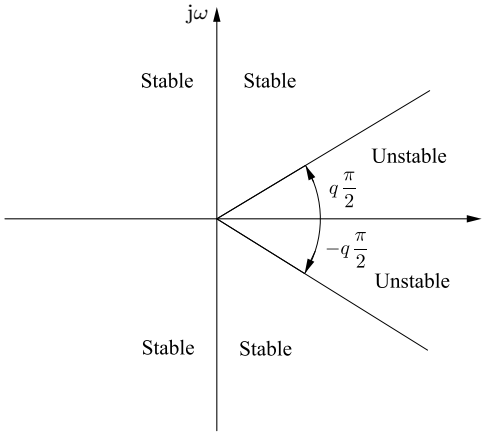


Fig. 2. Stability region of commensurate fractional-order system.

Table 1. Stability of equilibria of the fractional-order Lorenz-based chemical system (18).

Equilibrium points	Characteristic equations	Eigenvalues	Stability
$E_1 = (30,30,0)$	$\lambda^3 + 13.67\lambda^2 - 240.65\lambda - 719.75$	$\lambda_1 = -22.827$, $\lambda_2 = 11.827$, $\lambda_3 = -2.666$	unstable
$E_2 = (21.514,21.514,27)$	$\lambda^3 + 13.67\lambda^2 + 101.34\lambda + 1440.24$	$\lambda_1 = -13.854$, $\lambda_{2,3} = 0.094 \pm 10.195$i	unstable
$E_3 = (38.485,38.485,27)$	$\lambda^3 + 13.67\lambda^2 + 101.33\lambda + 1439.91$	$\lambda_1 = -13.854$, $\lambda_{2,3} = 0.093 \pm 10.194$i	unstable

4. Dynamical analysis of the fractional-order Lorenz-based chemical system

In this section, we study the dynamics of the fractional-order Lorenz-based chemical system (18). By varying the system parameters and fractional order, we can investigate the chaotic behavior of the system.

4.1. Dissipativity

We can write the system (18) in vector form as

$$ V = \begin{bmatrix} {}^{c}D_{t_0}^{q}x \\ {}^{c}D_{t_0}^{q}y \\ {}^{c}D_{t_0}^{q}z \end{bmatrix} = \begin{bmatrix} \alpha_2 y - \alpha_1 x \\ \alpha_3 x - \alpha_4 y + \alpha_5 z - \alpha_6 xz + \alpha_7 \\ -\alpha_8 x - \alpha_9 y - \alpha_{10} z + \alpha_{11} xy + \alpha_{12} \end{bmatrix}. \tag{32}$$

Thus, the divergence of vector field V is expressed as

$$ \begin{aligned} \nabla V &= \frac{\partial(\alpha_2 y - \alpha_1 x)}{\partial x} \\ &\quad + \frac{\partial(\alpha_3 x - \alpha_4 y + \alpha_5 z - \alpha_6 xz + \alpha_7)}{\partial y} \\ &\quad + \frac{\partial(-\alpha_8 x - \alpha_9 y - \alpha_{10} z + \alpha_{11} xy + \alpha_{12})}{\partial z} \\ &= -(\alpha_1 + \alpha_4 + \alpha_{10}). \end{aligned} \tag{33}$$

Since $\alpha_1 > 0$, $\alpha_4 > 0$, $\alpha_{10} > 0$, the system (18) is dissipative. Thus, the fractional-order system (18) has an attractor.

4.2. Bifurcation diagrams, Lyapunov exponent spectra and Poincaré map

The Lyapunov exponent is used to evaluate the exponential convergence or divergence of neighboring trajectories in a deterministic dynamical system. A positive Lyapunov exponent is a reliable sign of chaos. Based on the discrete formulas, the QR decomposition method is used to estimate the Lyapunov exponents of the fractional-order Lorenz-based chemical system (18).[51] The QR-factorization is applied to the Jacobian matrix $\boldsymbol{J}$ of the system in the following manner:

$$ \begin{aligned} & qr(\boldsymbol{J}_m \boldsymbol{J}_{m-1} \cdots \boldsymbol{J}_2 \boldsymbol{J}_1) \\ &= qr(\boldsymbol{J}_m \boldsymbol{J}_{m-1} \cdots \boldsymbol{J}_2 (\boldsymbol{J}_1 \boldsymbol{Q}_0)) \\ &= qr(\boldsymbol{J}_m \boldsymbol{J}_{m-1} \cdots \boldsymbol{J}_3 (\boldsymbol{J}_2 \boldsymbol{Q}_1))(\boldsymbol{R}_1) \\ &= qr(\boldsymbol{J}_m \boldsymbol{J}_{m-1} \cdots \boldsymbol{J}_4 (\boldsymbol{J}_3 \boldsymbol{Q}_2))(\boldsymbol{R}_2 \boldsymbol{R}_1) \end{aligned}$$

$$
\begin{aligned}
&= \cdots \\
&= qr(\boldsymbol{J}_m \boldsymbol{J}_{m-1} \cdots \boldsymbol{J}_{i+1}(\boldsymbol{J}_i \boldsymbol{Q}_{i-1}))(\boldsymbol{R}_{i-1}\boldsymbol{R}_{i-2}\cdots \boldsymbol{R}_2 \boldsymbol{R}_1) \\
&= \cdots \\
&= \boldsymbol{Q}_m(\boldsymbol{R}_m \boldsymbol{R}_{m-1}\cdots \boldsymbol{R}_2 \boldsymbol{R}_1) \\
&= \boldsymbol{Q}_m \boldsymbol{R}, \qquad (34)
\end{aligned}
$$

where $qr(\cdot)$ is the QR decomposition function. Thus, the Lyapunov exponent is calculated as

$$\lambda_j = \frac{1}{mh}\sum_{i=1}^{m} \ln|\boldsymbol{R}_i(j,j)|, \qquad (35)$$

where h is the step size.

Now, we study the influence of the derivative order on the dynamics of the Lorenz-based chemical system (18). Let $h = 0.001$, the iteration number $M = 20000$, and the parameter values as mentioned in Table 1. The bifurcation diagram and its corresponding Lyapunov exponent spectra are depicted in Figs. 3(a) and 3(b), respectively, when the derivative order ranges between $0.65 \le q \le 1$ with a step size of 0.01. From Fig. 3, the minimum derivative order in which the fractional-order system (18) exhibits chaotic behavior is 0.694. As we can observe, the maximum Lyapunov exponent (MLE) takes strictly positive values for $0.694 \le q \le 1$, meaning that the system (18) is in a chaotic state. Additionally, the unstable dynamics of system are confirmed by the finding of bifurcation diagram when the chaotic zone shifts to right as α_9 increases. Thus, we consider from this study that the lowest derivative order in which the fractional-order Lorenz-based chemical system (18) generates chaos is $q = 0.694$ by applying ADM.

Fix the system parameters as listed in Table 1 under the initial conditions $(x_0, y_0, z_0) = (32, 32, 32)$, phase portrait of the fractional-order Lorenz-based chemical system (18) is depicted in Fig. 4. As shown in Fig. 4(b), the chaotic attractor is not smooth, then the solution of the fractional-order system (18) is not accurate when $q = 0.694$ with iteration step size $h = 0.001$. To get smoother phase diagram, smaller h should be used in the simulation. In Fig. 4(c), $h = 0.0005$ is used for computer simulation and it is shown that a smooth chaotic attractor is obtained. Thus, in this case, the lowest derivative order to exhibit chaos is $q = 0.694$. Time-series of the states x, y, and z for $q = 0.694$ are shown in Fig. 5.

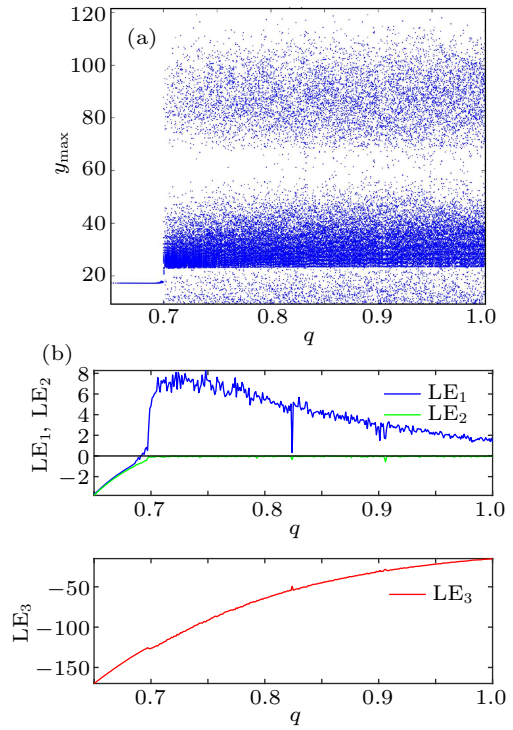


Fig. 3. Dynamics of the system (18) as q varies: (a) bifurcation diagram and (b) Lyapunov exponent spectra.

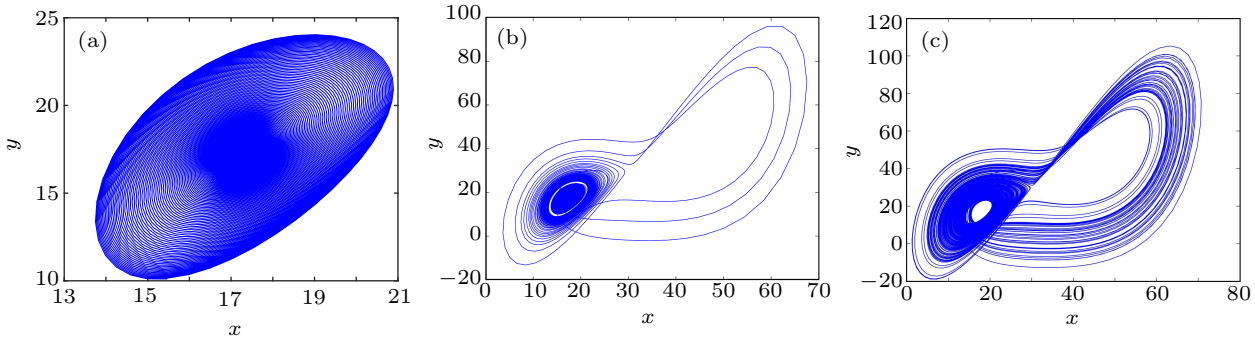


Fig. 4. Phase diagrams of the fractional-order Lorenz-based chemical system (18): (a) convergent state for $q = 0.693$; (b) chaotic attractor (not smooth) for $q = 0.694$ with $h = 0.001$; (c) chaotic attractor (smooth) for $q = 0.694$ with $h = 0.0005$.

A common phenomenon characterizes the chaotic systems, which is the sensitivity to initial conditions. A small change in the initial conditions can lead to completely different outcomes. In order to show this property in the chemical system (18), we select $q = 0.98$ and plot two trajectories with different initial conditions: $(x_0, y_0, z_0) = (32, 32, 32)$ and $(x_0, y_0, z_0) = (32.001, 32.001, 32.001)$, respectively. The results are illustrated in Fig. 6. As we can see, at the beginning, the time series are identical, but after a short time the difference between them is clear. Thus, we can conclude that the fractional-order Lorenz-based chemical system (18) is sensitive to initial conditions.

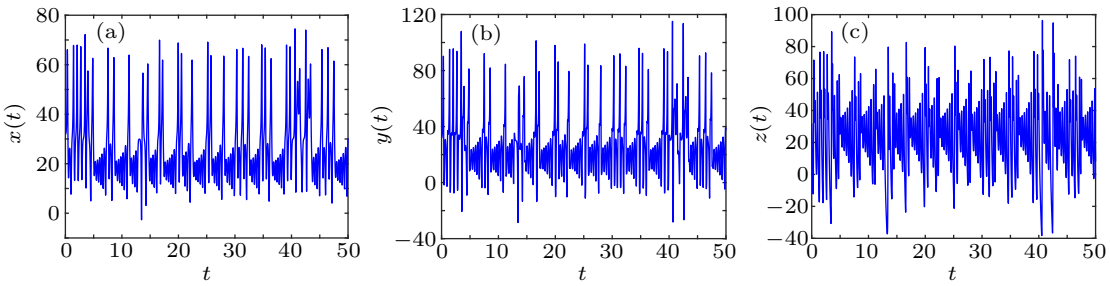


Fig. 5. (a) Time-series of the state x; (b) time-series of the state y; (c) time-series of the state z.

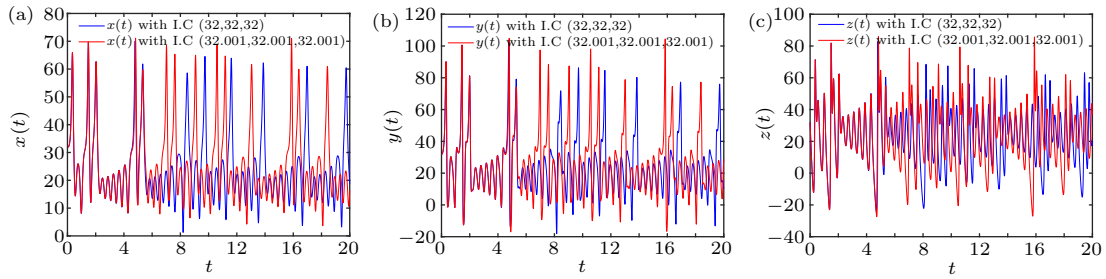


Fig. 6. Sensitive dependence on initial conditions for the fractional-order Lorenz-based chemical system (18).

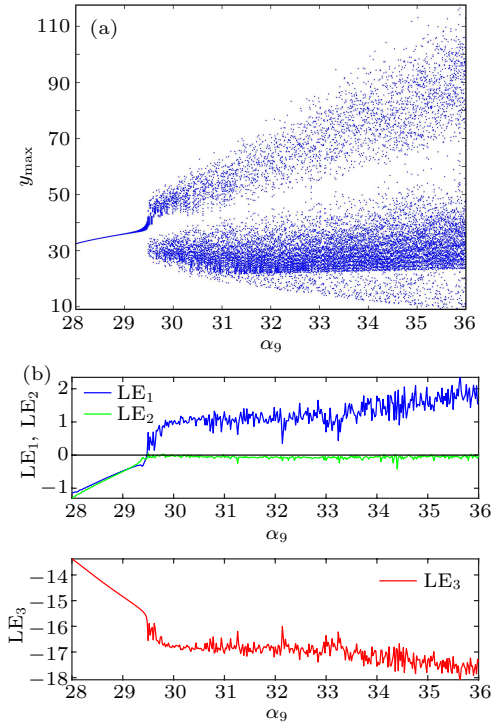


Fig. 7. Dynamics of the system (18) as α_9 varies: (a) bifurcation diagram and (b) Lyapunov exponent spectra.

Now, we study the influence of the system parameters on the dynamics of the system (18). We can choose any parameters among the system parameters. For example, we choose α_9 as the bifurcation parameter. Let $h = 0.001$, $q = 0.98$, and the system parameters as mentioned in Table 1, the bifurcation diagram and its corresponding Lyapunov exponent spectra when the parameter α_9 ranges between $28 \leq \alpha_9 \leq 36$ with a step size of 0.01 are shown in Figs. 7(a) and 7(b), respectively.

By examining the bifurcation diagram shown in Fig. 7(a), it can be seen that the dynamics of the system (18) are chaotic when α_9 varies between $29.52 \leq \alpha_9 \leq 36$, and in this case the chaotic zone shifts to the right as the system parameter α_9 increases. This finding is confirmed by the result of the maximum Lyapunov exponent in Fig. 7(b), in which the MLE takes positive values in this range, indicating that the system is in an unstable state.

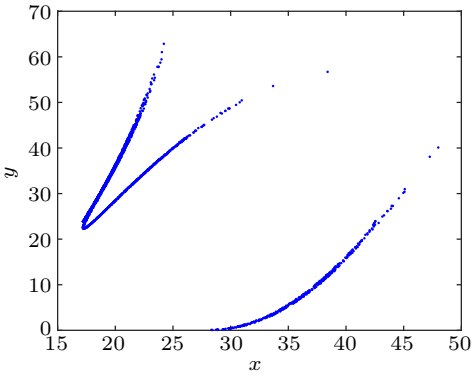


Fig. 8. A Poincaré map of the Lorenz-based chemical system (18).

In chaos theory, we can use the Poincaré map to study the bifurcation aspect and chaotic properties of a continuous dynamical system. For $q = 0.98$, a Poincaré map of the fractional-order Lorenz-based chemical system (18) obtained intersecting the orbit with the Poincaré section $z = 32$ is shown in Fig. 8. From this study, we can conclude that the fractional-order system (17) has rich dynamics.

5. The 0–1 test and complexity analysis of the fractional-order Lorenz-based chemical system

In this section, we study the complexity of the fractional-order Lorenz-based chemical system (18) and compare the results with the findings of bifurcation diagrams and Lyapunov exponent spectra.

5.1. The 0–1 test

In a deterministic dynamical system, the 0–1 test is an efficient method that allows us to determine whether or not the system exhibits chaotic dynamics. This powerful tool can determine if the dynamics of a system are regular or chaotic by means of a single scalar result, usually in the range $[0,1]$.[52] Based on a set of discrete data $x(n)$ selected from the fractional-order Lorenz-based chemical system (18), we define the translation variables $p(n)$ and $q(n)$ as follows:

$$p(n)=\sum_{i=1}^{n}\phi(i)\cos(\theta(i)),\quad q(n)=\sum_{i=1}^{n}\phi(i)\sin(\theta(i)),\tag{36}$$

where $\theta(i)=i\varphi+\sum_{j=1}^{i}\phi(j)$ and $\varphi\in[\frac{\pi}{5},\frac{4\pi}{5}]$ is a random constant. Furthermore, we plot the translation variables $p(n)$ and $q(n)$ in the p–q plane, in which the bounded trajectories imply regular dynamics, while the Brownian-like trajectories imply chaotic dynamics. Fix the system parameters as mentioned in Table 1 with $h=0.001$, Fig. 9 shows the dynamics of the translation variables $p(n)$ and $q(n)$ for different values of derivative order q.

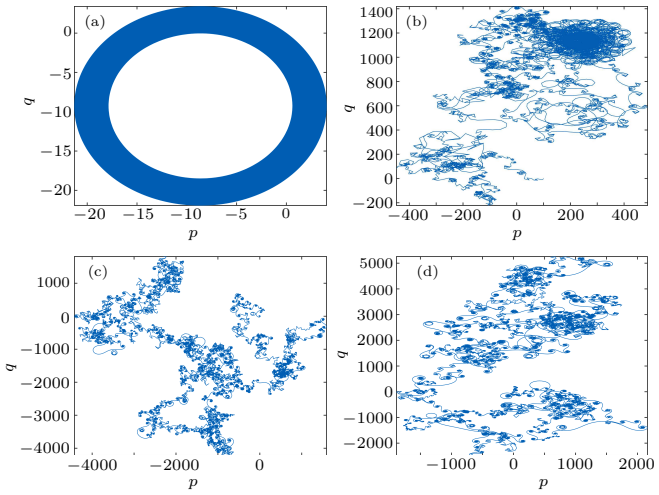


Fig. 9. The 0–1 test of the chemical system (18): (a) for $q=0.693$; (b) for $q=0.694$; (c) for $q=0.894$; (d) for $q=0.98$.

5.2. The C_0 complexity

The C_0 complexity algorithm is a numerical method based on the discrete Fourier transformation. It has significant importance and has produced good complexity analysis results in real-world applications due to its efficient and fast calculation speed. We use the C_0 complexity algorithm to measure the level of complexity of fractional-order Lorenz-based chemical system (18). Generally, the C_0 complexity algorithm is an indicator that can characterize the degree of randomness in discrete data. The implementation of this algorithm is as follows.

(I) Given a set of discrete data $x(n)$ $(n=1,2,\ldots,N)$ of length N from the system (18), the corresponding discrete Fourier transformation is given by

$$X(k)=\sum_{n=1}^{N}x(n)\exp\left[-\mathrm{j}\frac{2\pi nk}{N}\right],\tag{37}$$

where $k=1,2,\ldots,N$ and j is the imaginary unit.

(II) Taking the mean square value of $X(k)$ as

$$G_N=\frac{1}{N}\sum_{k=1}^{N}|X(k)|^2.\tag{38}$$

(III) Introducing a positive control parameter r such that

$$\tilde{X}(k)=\begin{cases}X(k), & \text{if}\quad |X(k)|^2>rG_N,\\ 0, & \text{if}\quad |X(k)|^2\le rG_N.\end{cases}\tag{39}$$

(IV) Next, the inverse Fourier transformation of $\tilde{X}(k)$ is given by

$$\tilde{x}(n)=\frac{1}{N}\sum_{k=1}^{N}\tilde{X}(k)\exp[\mathrm{j}\frac{2\pi nk}{N}],\tag{40}$$

where $n=1,2,\ldots,N$.

(V) Finally, the C_0 complexity is defined as[53]

$$C_0(r,N)=\frac{\sum_{n=1}^{N}|x(n)-\tilde{x}(n)|^2}{\sum_{n=1}^{N}|x(n)|^2}.\tag{41}$$

We adopt the C_0 complexity algorithm to explore the chaotic dynamics in the system (18). Fix the system parameters as mentioned in Table 1, let the derivative order q vary from 0.65 to 1 with a step size of 0.01. The C_0 complexity of the fractional-order system (18) is represented in Fig. 10.

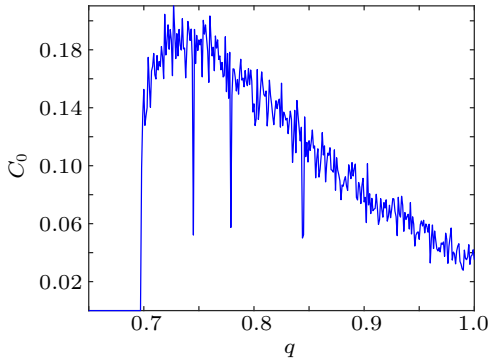


Fig. 10. The C_0 complexity of the chemical system (18) versus q.

As shown in Fig. 10, the complexity of the fractional-order Lorenz-based chemical system (18) has a high level when the derivative order ranges between $0.694\le q\le 1$, meaning that the fractional-order system (18) is in a chaotic state, whereas the complexity of the system approaches 0 for $0.65\le q<0.694$, meaning that the system's dynamics are stable, which agrees well with the findings of 0–1 test, bifurcation diagram, and maximum Lyapunov exponent.

In order to show the sensitivity of the system (18) to variation of its parameters and derivative order simultaneously, we plot the chaos diagrams in the plane. In practice, we can use the chaos diagram to select the parameters if a more complex structure is required in real-world applications. A chaos diagram of the fractional-order system (18) based on C_0 complexity, where the derivative order q ranges between $0.65\le q\le 1$ with a step size of 0.01, and the parameter α_9 ranges between $29.5\le\alpha_9\le 36$ with a step size of 0.05 is illustrated in Fig. 11.

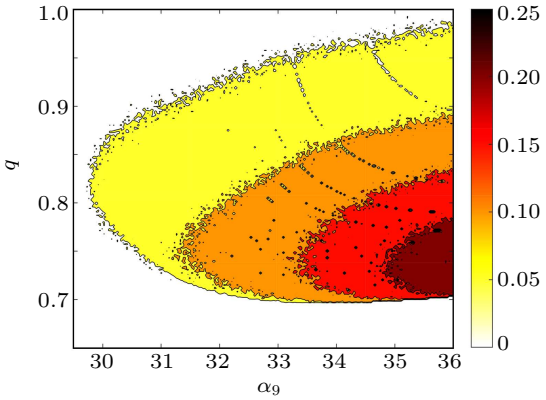


Fig. 11. Chaos diagram based on C_0 complexity in the q–α_9 plane.

From Fig. 11, it is shown that the complexity of the chemical system (18) changes according to the derivative order q and parameter α_9 values. A high complexity level has been obtained when the derivative order q is greater than 0.694 and the parameter α_9 approaches 35.5, meaning that the system has complex dynamics, which agrees with our selection of parameter values and derivative order in this paper.

6. Modified projective synchronization of the fractional-order Lorenz-based chemical system

Based on the Lyapunov stability theory of fractional-order dynamical systems, a modified projective synchronization of chaotic systems is presented in this section.

6.1. Theoretical analysis

Consider the drive chaotic system described by

$$ {}^{c}D_{t_0}^{q}X = F(X), \tag{42}$$

where the state vector $X=(x_1,x_2,\ldots,x_n)^{\mathrm{T}}$. Assuming that the response chaotic system can be expressed as

$$ {}^{c}D_{t_0}^{q}Y = CY + g(Y) + U, \tag{43}$$

where the state vector $Y=(y_1,y_2,\ldots,y_n)^{\mathrm{T}}$, $C\in\mathbb{R}^{n\times n}$, $g(Y)$ is the nonlinear part, and $U=(u_1,u_2,\ldots,u_n)^{\mathrm{T}}$ is the controller.

Definition 3 For the drive system (42) and the response system (43), it is said to achieve MPS if there exists a controller U such that $\lim_{t\to\infty}\|Y(t)-\Lambda X(t)\|=0$, where $\Lambda\in\mathbb{R}^{n\times n}$ is a diagonal matrix, i.e., $\Lambda=\mathrm{diag}(\beta_1,\beta_2,\ldots,\beta_n)$, and $\beta_j\neq 0$ for $j=1,2,\ldots,n$.

Remark 1 The matrix Λ is called the scaling matrix, and $\beta_j\,(j=1,2,\ldots,n)$ are real numbers called the scaling factors.

If $\beta_j=1$ ($\beta_j=-1$, respectively) for $j=1,2,\ldots,n$, MPS is reduced to complete synchronization (anti-synchronization, respectively).

Our goal is to construct an efficient controller U, in which the trajectories of the response chaotic system asymptotically track the trajectories of the drive chaotic system in the sense of MPS. First, we give the following theorem.

Theorem 2 For a given real scaling matrix and any initial conditions, the MPS between systems (42) and (43) can be achieved under the following control law:

$$ U=(\tilde{C}-K)\boldsymbol{e}-CY-g(Y)+\Lambda F(X), \tag{44}$$

where $\tilde{C}\in\mathbb{R}^{n\times n}$ is a diagonal matrix that has the same diagonal elements as the matrix C. $K\in\mathbb{R}^{n\times n}$ is a control gain matrix that satisfies $|\arg(\lambda_j(\tilde{C}-K))|>q\frac{\pi}{2}$ for $j=1,2,\ldots,n$. Here, we denote by $\lambda_j(A)$ the set of eigenvalues of the matrix A.

Proof Let us define the MPS error between the systems (42) and (43) as

$$ \boldsymbol{e}=Y-\Lambda X. \tag{45}$$

Thus, the error dynamics are easily obtained as

$$\begin{aligned} {}^{c}D_{t_0}^{q}\boldsymbol{e} &= {}^{c}D_{t_0}^{q}(Y-\Lambda X)={}^{c}D_{t_0}^{q}Y-\Lambda\,{}^{c}D_{t_0}^{q}X \\ &= CY+g(Y)-\Lambda F(X)+U. \end{aligned} \tag{46}$$

Substituting Eq. (44) into Eq. (46) yields

$$ {}^{c}D_{t_0}^{q}\boldsymbol{e}=(\tilde{C}-K)\boldsymbol{e}. \tag{47}$$

We have $|\arg(\lambda_j(\tilde{C}-K))|>q\frac{\pi}{2}$ for $j=1,2,\ldots,n$, according to the Lyapunov stability theory, the error vector $\boldsymbol{e}$ converges asymptotically towards zero as $t\to\infty$. Hence, the drive and response systems in Eqs. (42) and (43) are synchronized in the sense of MPS under the controller (44). The proof is complete.

6.2. MPS of the fractional-order Lorenz-based chemical system

To illustrate the feasibility of the proposed MPS method, we consider the fractional-order Lorenz-based chemical system (18) as an example of synchronization. Thus, the drive and response chaotic systems are described by

$$\begin{aligned} \begin{pmatrix} {}^{c}D_{t_0}^{q}x_m \\ {}^{c}D_{t_0}^{q}y_m \\ {}^{c}D_{t_0}^{q}z_m \end{pmatrix} &= \begin{bmatrix} -\alpha_1 & \alpha_2 & 0 \\ \alpha_3 & -\alpha_4 & \alpha_5 \\ -\alpha_8 & -\alpha_9 & -\alpha_{10} \end{bmatrix} \begin{pmatrix} x_m \\ y_m \\ z_m \end{pmatrix} \\ &\quad + \begin{pmatrix} 0 \\ -\alpha_6 x_m z_m+\alpha_7 \\ \alpha_{11}x_m y_m+\alpha_{12} \end{pmatrix}, \\ \begin{pmatrix} {}^{c}D_{t_0}^{q}x_s \\ {}^{c}D_{t_0}^{q}y_s \\ {}^{c}D_{t_0}^{q}z_s \end{pmatrix} &= \begin{bmatrix} -\alpha_1 & \alpha_2 & 0 \\ \alpha_3 & -\alpha_4 & \alpha_5 \\ -\alpha_8 & -\alpha_9 & -\alpha_{10} \end{bmatrix} \begin{pmatrix} x_s \\ y_s \\ z_s \end{pmatrix} \\ &\quad + \begin{pmatrix} 0 \\ -\alpha_6 x_s z_s+\alpha_7 \\ \alpha_{11}x_s y_s+\alpha_{12} \end{pmatrix} + \begin{pmatrix} u_1 \\ u_2 \\ u_3 \end{pmatrix}, \end{aligned} \tag{48}$$

where the subscripts of m and s denote the drive system and response system, respectively. $U=(u_1,u_2,u_3)^{\mathrm{T}}$ is the controller. According to Eq. (43), we obtain

$$ C=\begin{bmatrix} -\alpha_1 & \alpha_2 & 0 \\ \alpha_3 & -\alpha_4 & \alpha_5 \\ -\alpha_8 & -\alpha_9 & -\alpha_{10} \end{bmatrix}, $$

$$g(x,y,z)=\begin{pmatrix}0\\-\alpha_6 xz+\alpha_7\\ \alpha_{11}xy+\alpha_{12}\end{pmatrix}. \tag{49}$$

Next, the synchronization error is defined as

$$\begin{cases} e_1 = x_s-\beta_1 x_m,\\ e_2 = y_s-\beta_2 y_m,\\ e_3 = z_s-\beta_3 z_m, \end{cases} \tag{50}$$

where $\Lambda=\mathrm{diag}(\beta_1,\beta_2,\beta_3)$ is the scaling matrix with $\beta_j\neq 0$ for $j=1,2,3$. Using Eq. (48), the error dynamical system is obtained as

$$\begin{cases} {}^cD^q_{t_0}e_1 = -\alpha_1 e_1+\alpha_2(y_s-\beta_1 y_m)+u_1,\\ {}^cD^q_{t_0}e_2 = -\alpha_4 e_2+\alpha_3(x_s-\beta_2 x_m)+\alpha_5(z_s-\beta_2 z_m)\\ \qquad -\alpha_6 x_s z_s+\beta_2\alpha_6 x_m z_m+(1-\beta_2)\alpha_7+u_2,\\ {}^cD^q_{t_0}e_3 = -\alpha_{10}e_3-\alpha_8(x_s-\beta_3 x_m)-\alpha_9(y_s-\beta_3 y_m)\\ \qquad +\alpha_{11}x_s y_s-\beta_3\alpha_{11}x_m y_m+(1-\beta_3)\alpha_{12}+u_3. \end{cases} \tag{51}$$

According to theorem 2, the controllers u_j $(j=1,2,3)$ are constructed as

$$\begin{cases} lu_1 = -\alpha_2(y_s-\beta_1 y_m)-k_1 e_1,\\ u_2 = -\alpha_3(x_s-\beta_2 x_m)-\alpha_5(z_s-\beta_2 z_m)\\ \qquad +\alpha_6 x_s z_s-\beta_2\alpha_6 x_m z_m-(1-\beta_2)\alpha_7-k_2 e_2,\\ u_3 = \alpha_8(x_s-\beta_3 x_m)+\alpha_9(y_s-\beta_3 y_m)-\alpha_{11}x_s y_s\\ \qquad +\beta_3\alpha_{11}x_m y_m-(1-\beta_3)\alpha_{12}-k_3 e_3, \end{cases} \tag{52}$$

where $K=\mathrm{diag}(k_1,k_2,k_3)$ is the control gain matrix. Substituting Eq. (52) into Eq. (51), the error dynamical system can be simplified as

$$\begin{aligned}\begin{pmatrix}{}^cD^q_{t_0}e_1\\ {}^cD^q_{t_0}e_2\\ {}^cD^q_{t_0}e_3\end{pmatrix} &= \begin{bmatrix}-(\alpha_1+k_1) & 0 & 0\\ 0 & -(\alpha_4+k_2) & 0\\ 0 & 0 & -(\alpha_{10}+k_3)\end{bmatrix}\begin{pmatrix}e_1\\ e_2\\ e_3\end{pmatrix}\\ &= (\tilde{C}-K)\boldsymbol{e}, \end{aligned} \tag{53}$$

where

$$\tilde{C}=\begin{bmatrix}-\alpha_1 & 0 & 0\\ 0 & -\alpha_4 & 0\\ 0 & 0 & -\alpha_{10}\end{bmatrix}. \tag{54}$$

If the control gain matrix K is selected so that $|\arg(\lambda_j(\tilde{C}-K))|>q\frac{\pi}{2}$ $(j=1,2,3)$, according to the stability theory of fractional-order systems, the trivial solution of the dynamical error system (53) is asymptotically stable. Therefore, the MPS between the chaotic systems is achieved.

For the computer simulations, the system parameters are taken as listed in Table 1 and the derivative order is selected as $q=0.98$, and then the fractional-order system (18) is chaotic. We select the initial states of the drive and response systems as $(x_m(0),y_m(0),z_m(0))=(32,32,32)$, and $(x_s(0),y_s(0),z_s(0))=(12,18,24)$, respectively. Also, we take the scaling matrix as $\Lambda=\mathrm{diag}(1.5,-0.5,-2)$ and the control gain matrix as $K=\mathrm{diag}(0,1,1/3)$. Hence, the eigenvalues of the matrix $(\tilde{C}-K)$ are obtained as $\lambda_1=-10$, $\lambda_2=-2$, $\lambda_3=-3$, then we have $|\arg(\lambda_j)|=\pi>q\frac{\pi}{2}$ for $j=1,2,3$, and the stability condition is satisfied. The simulation results of the proposed synchronization technique are shown in Figs. 12 and 13. Figure 12 represents the three-dimensional projection of chaotic attractors of the drive and response systems described in Eq. (48). In Figs. 13(a)–13(c), we show the time-series of states when the MPS occurs, whereas Fig. 13(d) depicts the evolution of the MPS error $\boldsymbol{e}=(e_1,e_2,e_3)^{\mathrm{T}}$ which converges towards zero as $t\to\infty$. Hence, the MPS between the chaotic systems is obtained under the designed controller (52).

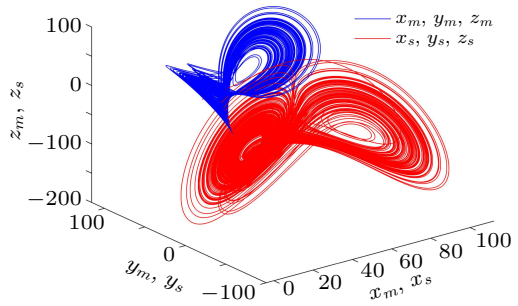


Fig. 12. Three-dimensional projection of the chaotic attractors of the drive and response systems for $q=0.98$.

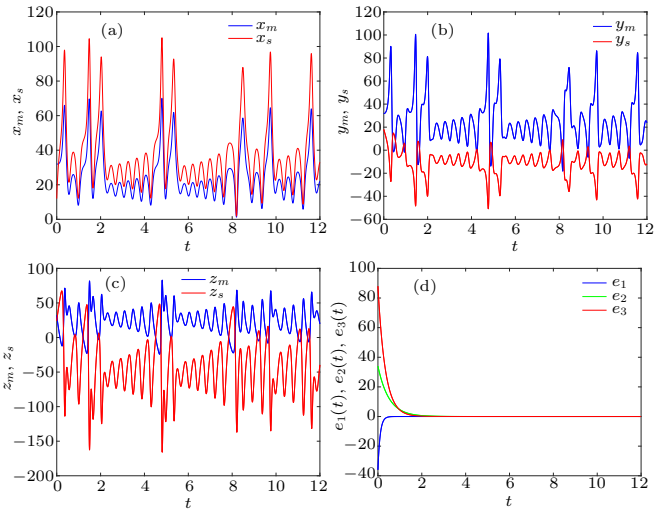


Fig. 13. Simulation results of MPS of the chaotic chemical system (18): (a) time series of x_m and x_s; (b) time series of y_m and y_s; (c) time series of z_m and z_s; (d) time-history of the synchronization errors.

7. Realization of secure communication

7.1. A general method for secure communication scheme based on MPS of chaotic systems

Recently, researchers and engineers have shown significant progress in using chaotic systems for secure communication. By exploiting the qualitative properties of chaotic systems, a high security level is gained when the information signal is transmitted. In this section, the application of MPS of

the chaotic systems in secure communication is investigated. The block diagram of our secure communication scheme based on chaotic modulation is shown in Fig. 14, where the fractional-order chaotic system (18) is considered as the transmitter and receiver systems in the proposed scheme. U is the designed controller for synchronization. In the transmitter, we modulate the information signal $m(t)$ into the chaotic signal by employing an invertible function $\Phi(x_m, y_m, z_m, m(t))$, which is defined by $m'(t) = \Phi(x_m, y_m, z_m, m(t))$. Next, the signal $m'(t)$ is injected into one of the three variables x_m, y_m, and z_m. Assuming, for instance, that the signal $m'(t)$ is mixed with the variable x_m and derives a combined signal $\vartheta(t) = x_m(t) + m'(t)$, which is transmitted with x_m, y_m, and z_m to the receiver through the channel. In the receiver, the MPS between the drive and response chaotic systems is obtained by employing the designed controller U. So, the state x_s will approach to $\beta_1 x_m$. Hence, the signal $m'(t)$ can be extracted via the transformation $m'(t) = \vartheta(t) - x_s/\beta_1$. Finally, the information signal $m(t)$ can be recovered by $m(t) = \Phi^{-1}(x_s, y_s, z_s, m'(t))$.

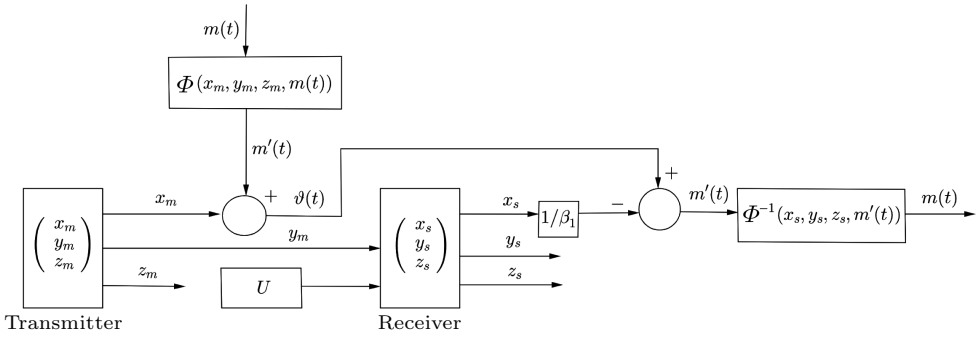


Fig. 14. Block diagram of the proposed chaos-based secure communication system.

7.2. Numerical simulations

To illustrate the previous theoretical method, MATLAB simulations are provided in this paper. First, we select the system parameters, the initial states of the transmitter and receiver systems, the derivative order, the scaling matrix, and the control gain matrix as in Section 6. Thus, the MPS between the chaotic systems is achieved. The information signal $m(t)$ is taken as a sinusoidal signal $m(t) = 20\sin(2\pi t/3)$, and the transformation Φ is selected as $m'(t) = y_m + m(t)$. Here, $m'(t)$ is assumed to be injected into the variable x_m. Figure 15 illustrates the simulation process. The information signal $m(t)$ and the transmitted signal $\vartheta(t)$ are depicted in Figs. 15(a) and 15(b), respectively. The recovered signal $\tilde{m}(t)$ is shown in Fig. 15(c). Figure 15(d) illustrates the error between the original signal and the recovered one. From Fig. 15(d), it can be observed that the error of the transmitted information converges towards zero as $t \to \infty$, and then the original signal can be successfully recovered.

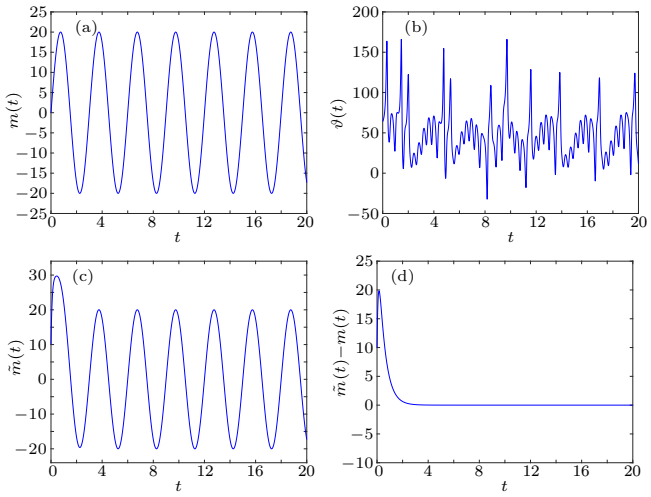


Fig. 15. Secure communication results based on the MPS of chaotic systems. An example of a sinusoidal signal: (a) the original signal $m(t)$; (b) the transmitted signal $\vartheta(t)$; (c) the recovered signal $\tilde{m}(t)$; (d) the error signal $\tilde{m}(t) - m(t)$.

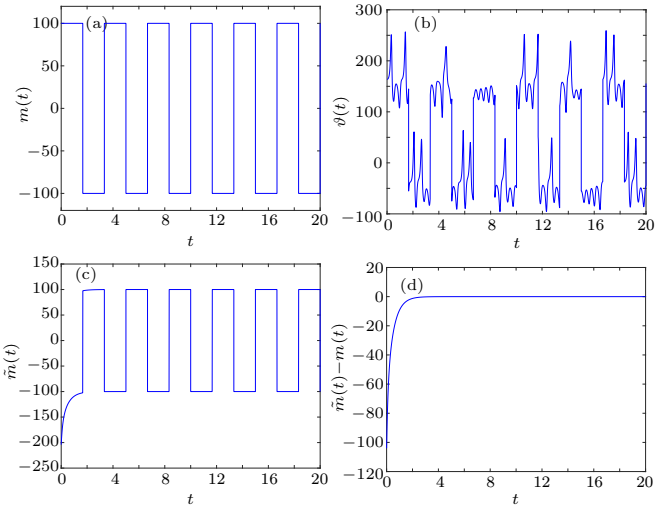


Fig. 16. Secure communication results based on the MPS of chaotic systems. An example of a square wave: (a) the original information signal $m(t)$; (b) the transmitted signal $\vartheta(t)$; (c) the recovered signal $\tilde{m}(t)$; (d) the error signal $\tilde{m}(t) - m(t)$.

To better demonstrate the accuracy of the constructed chaos-based secure communication scheme, we take the original signal as a square wave. Here, the transformation Φ is selected as $m'(t) = x_m + m(t)$ and inject $m'(t)$ into the variable y_m. Figure 16 illustrates the simulation process. Figures 16(a)

and 16(b) depict the original signal $m(t)$ and the transmitted signal $\vartheta(t)$, respectively. Figure 16(c) represents the recovered signal $\tilde{m}(t)$. Figure 16(c) shows that the recovered signal $\tilde{m}(t)$ coincides with high accuracy with the original signal $m(t)$ after a brief transitional period. As shown in Fig. 16(d), the error signal $\tilde{m}(t) - m(t)$ converges towards zero in infinite time, which validates the feasibility of our secure communication scheme.

8. Conclusions and future works

Two main objectives have been gained from this research study. The first objective was to investigate the dynamics properties of the fractional-order Lorenz-based chemical system using powerful nonlinear tools, such as phase plots, bifurcation diagrams, Lyapunov exponent spectra, and chaos diagrams. In addition, the complexity of the fractional-order system has been analyzed based on the C_0 algorithm. The second objective was to achieve a chaos synchronization between two identical fractional-order systems, where the MPS method is illustrated. As a result, a secure communication scheme based on the MPS of fractional-order chaotic systems has been developed. Computer simulations were provided in this research paper to verify the validity and effectiveness of the chaotic synchronization method and secure communication scheme. Regarding open research problems, chaos-based image encryption is an important topic related to the applications of chaotic systems. Our future plan is to focus our efforts on this topic because we believe that developing new image encryption algorithms might help engineers provide robust security in practical applications, including medical and satellite fields.

References

[1] Bekir A and Zahran E H 2022 *Chin. Phys. B* **31** 060401
[2] Ding D, Niu Y, Zhang H, Yang Z, Wang J, Wang W and Wang M 2024 *Chin. Phys. B* **33** 050503
[3] Bukhari A H, Raja M A Z, Shoaib M and Kiani A K 2022 *Chaos, Solitons Fractals* **161** 112375
[4] Chaudhary M and Singh M K 2022 *Phys. Scr.* **97** 074001
[5] Farman M, Akgül A, Saleem M U, Imtiaz S and Ahmad A 2020 *Pramana* **94** 1
[6] AbdelAty A M, Al-Durra A, Zeineldin H and El-Saadany E F 2024 *Int. J. Electr. Power Energy Syst.* **156** 109746
[7] Rajagopal K, Karthikeyan A and Ramakrishnan B 2021 *Chin. Phys. B* **30** 120512
[8] Pahnehkolaei S M A, Alfi A and Machado J T 2022 *Chaos, Solitons Fractals* **155** 111658
[9] Cafagna D and Grassi G 2015 *Chin. Phys. B* **24** 080502
[10] Khennaoui A A, Ouannas A, Bendoukha S, Wang X and Pham V T 2018 *Entropy* **20** 530
[11] Podlubny I 2009 *Fractional Differential Equations* (New York: Academic Press)
[12] Caputo M and Fabrizio M 2015 *Prog. Fract. Differ. Appl.* **1** 73
[13] Atangana A and Baleanu D 2016 *Therm. Sci.* **20** 763
[14] He S, Wang H and Sun K 2022 *Chin. Phys. B* **31** 060501
[15] Atangana A and Secer A 2013 *Abstr. Appl. Anal.* **2013** 279681
[16] Strogatz S H 2018 *Nonlinear dynamics and chaos: with applications to physics, biology, chemistry, and engineering* (Boca Raton: CRC press)
[17] Hannachi F 2019 *SN Appl. Sci.* **1** 158
[18] Kocamaz U E, Wang H and Uyaroğlu Y 2014 *Nonlinear Dyn* . **75** 63
[19] Aqeel M, Azam A and Ayub J 2022 *Chin. J. Phys.* **77** 1331
[20] Bodale I and Oancea V A 2015 *Chaos Solitons Fractals* **78** 1
[21] Yadav V K, Das S, Bhadauria B S, Singh A K and Srivastava M 2017 *Chin. J. Phys.* **55** 594
[22] He S, Sun K and Banerjee S 2016 *Eur. Phys. J. Plus* **131** 1
[23] Dou G, Liu J, Zhang M, Zhao K and Guo M 2022 *Eur. Phys. J. Plus* **231** 3151
[24] Kheiri H and Naderi B 2015 *Iranian J. Math. Chem.* **6** 81
[25] Garcia-Fernández J M, Nieto-Villar J M and Rieumont-Briones J 1996 *Phys. Scr.* **53** 643
[26] Carroll T L and Pecora L M 1990 *Phys. Rev. Lett.* **64** 821
[27] Sang J Y, Yang J and Yue L J 2011 *Chin. Phys. B* **20** 080507
[28] Shukla V K, Joshi M C, Rajchakit G, Chakrabarti P, Jirawattanapanit A and Mishra P K 2023 *Differ. Equ. Dyn. Syst.* **20** 1
[29] Ling L, Yuan C and Ling L 2010 *Chin. Phys. B* **19** 080506
[30] Grassi G 2012 *Chin. Phys. B* **21** 050505
[31] Gholizade-Narm H, Azemi A and Khademi M 2013 *Chin. Phys. B* **22** 070502
[32] Zhu Y R, Wang J L and Han X 2024 *Neurocomputing* **591** 127766
[33] Du H, Zeng Q, Wang C and Ling M 2010 *Nonlinear Anal. Real World Appl.* **11** 705
[34] Du H, Zeng Q and Wang C 2009 *Chaos Solitons Fractals* **42** 2399
[35] Li G H 2007 *Chaos Solitons Fractals* **32** 1786
[36] Haneche N and Hamaizia T 2024 *Phys. Scr.* **90** 095203
[37] Wu X, Fu Z and Kurths J 2015 *Phys. Scr.* **90** 045210
[38] Khan A, Nigar U and Chaudhary H 2022 *Int. J. Appl. Comput. Math* **8** 170
[39] Benkouider K, Bouden T and Yalcin M E 2020 *SN Appl. Sci.* **2** 1
[40] Bonny T, Nassan W A, Vaidyanathan S and Sambas A 2023 *Multimed Tools Appl.* **82** 34229
[41] Wu X, Wang H and Lu H 2012 *Nonlinear Anal. Real World Appl.* **13** 1441
[42] Liu M, Yu W, Wang J, Gao K and Zhou Z 2023 *Int. J. Dynam. Control* **11** 1952
[43] Gorenflo R and Mainardi F 1997 *Fractal and Fractional Calculus in Continuum Mechanics* (Wien: Springer)
[44] Andrew L Y T, Li X F, Chu Y D and Hui Z 2015 *Chin. Phys. B* **24** 100502
[45] He S, Sun K and Wang H 2016 *Math. Meth. Appl. Sci.* **39** 2965
[46] Shi K, An X, Xiong L, Yang F and Zhang L 2022 *Phys. Scr.* **97** 045201
[47] Fu H and Lei T 2022 *Symmetry* **14** 484
[48] Lorenz E N 1963 *Journal of Atmospheric Sciences* **20** 130
[49] Poland D 1993 *Phys. D* **65** 86
[50] Matignon D 1996 *Computational Engineering in Systems and Applications* **2** 963
[51] Li C, Gong Z, Qian D and Chen Y 2010 *Chaos* **20** 013127
[52] Sun K H, Liu X and Zhu C X 2010 *Chin. Phys. B* **19** 110510
[53] Wang S, He S, Yousefpour A, Jahanshahi H, Repnik R and Perc M 2020 *Chaos Solitons Fractals* **131** 109521